IEEE Access
Multidisciplinary | Rapid Review | Open Access Journal

Received July 2, 2020, accepted July 13, 2020, date of publication July 16, 2020, date of current version July 28, 2020.

*Digital Object Identifier 10.1109/ACCESS.2020.3009754*

# Analysis and Modeling of the Forces Exerted on the Cookware in Induction Heating Applications

**JESÚS ACERO[1], (Senior Member, IEEE), IGNACIO LOPE[2,3], (Member, IEEE), CLAUDIO CARRETERO[2], (Senior Member, IEEE), AND JOSÉ M. BURDÍO[1], (Senior Member, IEEE)**

[1]Department of Electronic Engineering and Communications, University of Zaragoza, 50018 Zaragoza, Spain
[2]Department of Applied Physics, University of Zaragoza, 50009 Zaragoza, Spain
[3]B/S/H/ Home Appliances, 50016 Zaragoza, Spain

Corresponding author: Jesús Acero (jacero@unizar.es)

This work was partly supported by the Spanish MICINN under Project PID2019-103939RB-I00, by the Spanish MICINN and AEI under Project RTC-2017-5965-6, co-funded by EU through FEDER program, and by the BSH Home Appliances Group.

**ABSTRACT** We present a semianalytical model for calculating the forces exerted on cookware in domestic induction heating applications. The developed model is based on the Maxwell's stress tensor and is also based on the existing semianalytic expressions of the electromagnetic fields in planar induction heating systems, which are expressed in terms of Fourier-Bessel series. Taking advantage of the axial symmetry of usual domestic induction heating systems, the flux of the vertical component of the Maxwell's stress tensor is analytically integrated and the vertical force is obtained. The proposed model captures both eddy currents and magnetization that occurs in typical ferromagnetic cookware. The model is verified by means of two-dimensional Finite Element simulations and also is tested by means of measurements of the change of the weight experimented by cookware due to the forces during the heating process.

**INDEX TERMS** Induction heating, appliances, electromagnetic forces, Maxwell's stress tensor, electromagnetic properties.

## I. INTRODUCTION

Induction heating cooktops have progressively gained the interest of users due to its intrinsic advantages, as contactless heat transfer, automatic cookware detection, fast operation and high efficiency, which outperforms the traditional cooking stoves [1]. Currently, induction cooktops are technologically advanced products whose mentioned advantages compensate its extra cost with respect to gas or radiant burners. The research and development efforts conducted in the last years have been focused on the enabling technologies of induction cooktops: magnetics [2]–[7], power electronics converters [8]–[10], digital controllers, modelling and control [11]–[13]. These efforts have been reflected in more accurate control, safer operation and faster appliances.

The high efficiency achieved with induction cookers and ferromagnetic pots is attracting a considerable number of users concerned by environmental aspects. In a domestic induction heating process the heat is generated in the workpiece. This is efficient by nature because neither external heat sources nor heat transmission media are required. For this reason, in current arrangements the efficiency of the energy transfer can be up to 97.5% for the case of ferromagnetic cookware [14]. In the case of non-ferromagnetic materials (copper or aluminum) efficiencies comprised between $60\% - 70\%$ can be reached.

Currently, the approach of manufacturers is moving towards the improvement of the cooking experience of users [15], [16]. In this way, advanced induction heating appliances incorporate innovations, as connectivity to other devices, self-guided helping for preparing recipes, and automatic cooking functionalities. In general, the two last innovations require measurements of the weight and the temperature of the pot during the cooking process. However, due to the inductive nature of heating, the weight measurement is more complex than temperature measurement because the pot is under electromagnetic forces which depend on several aspects as power level, materials and size of the cookware, and the inductor system arrangement. Therefore, accurate weight measurements should take into account the force

The associate editor coordinating the review of this manuscript and approving it for publication was N. Prabaharan.

between the cookware and the inductor system. Literature has echoed this issue and some contributions have been presented in order to reduce or optimize the mentioned forces [17], [18].

Usually, the analysis and modeling of domestic induction heating systems has been inspired by other related applications. However, the application of related models to this case is not, in general, straightforward. Industrial induction heating applications have the same nature of domestic induction heating. However, industrial induction heating presents several differences with respect to domestic applications. In industrial applications the coil geometry is usually solenoidal, whereas domestic applications uses flat coils. Moreover, non-ferromagnetic materials are mainly used as workpieces in industrial applications, and the phenomenology associated to the magnetic permeability of the ferromagnetic cookware is not present. The nature of the electromechanical force in cookware an the forces existing in electrical machines is essentially the same. However, domestic induction heating applications presents two distinct characteristics with respect to the electrical machines. The first characteristic is due to the properties of usual cookware materials, which combine both electrical conductivity and magnetic permeability. Consequently, the cookware is simultaneously the path of the magnetic flux the path of the induced currents. However, in electrical machines flux and current paths are usually separated in the core (yoke) and the windings, and eddy currents are tried to be avoided in cores by using different strategies. Second, operating frequencies are usually orders of magnitude higher in induction heating than electrical machines.

This work is aimed at obtained an analytical model of the forces in domestic induction heating applications. For this purpose, models existing in the literature are first reviewed. In general, two main approaches have been followed for calculating forces in electromechanical applications: finite element (FEA) simulations and analytical models. FEA approaches have been extensively used for analyzing both electrical machines [19]–[22] and industrial induction heating applications [23]–[26]. Considering domestic induction applications and FEA approaches, a preliminary analysis of forces on the cookware was presented in [27]. Results pointed that the total force has two components, in opposite directions, whose value depends on the electrical conductivity and the magnetic permeability of the cookware. A FEA approach is also followed in the above mentioned references [17], [18] The first reference proposes a new coil structure for reducing the force and the second reference proposes a coil structure for optimizing the force in a levitating induction cooker. In both works, two-dimensional (2D) finite element simulations are used for obtaining the forces on the cookware.

Analytical or semianalytical models are effective for study the effect of different parameters on the electromagnetic magnitudes of a system. Generally, in analytical approaches the field magnitudes are obtained from the magnetic scalar or vector potentials and, subsequently, parameters as impedance, emf or forces are calculated by integrating or by means of the Maxwell's stress tensor. In general, an analytical model can only be obtained if the system under study presents symmetry because it allows to simplify the problem. In the case of electrical machines, some analytical models for calculating forces were proposed by applying symmetry [28]–[33]. Regarding industrial applications, analytical models were proposed in the past for obtaining the forces in elongated systems with cylindrical symmetry [34], [35]. However, similar models for planar induction systems are not found in the current literature.

Fig. 1 illustrates a typical arrangement of a domestic induction system. This system basically has cylindrical symmetry and this characteristic was used in the past to derive a semianalytical model of the fields [36], which allowed to obtain a model of the equivalent impedance [37] and the inductive efficiency [14]. At the interest frequency range (from 20 kHz to 100 kHz) the equivalent impedance consists of the series connection of equivalent resistor and inductor, whose values depend on the characteristics of the system and the operating frequency. The resistance represents the power dissipation in the different elements (cookware, windings, shielding) and the inductance represents the existing magnetic field in the system. The equivalent impedance can be obtained by means of both FEA approaches or analytical models. Ferrite bars improve the coupling between the windings and the cookware and they play a similar role of the core in inductors and transformers. Despite Fig. 1 shows a 3D system, its high symmetry has favoured the analysis by means 2D simulations or analytical solutions because both strategies reduce the development time and the required computational resources. However, the suitability of 2D approaches should be confirmed by means of experiments.

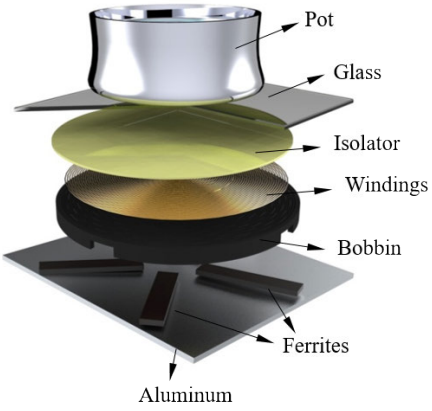


**FIGURE 1.** Basic induction heating system comprising the planar windings, ferrites, aluminum shielding and vessel.

Considering this previous semianalytical solution, in this paper a model of the force exerted on the cookware heated by induction is contributed with respect to previous works. The model is verified by means of a double test. First, 2D Finite Element (FEA) simulations, and second, experiments where

the weight of a cookware during a cooking process is recorded by means of several load cells and a data logger.

The paper is organized as follows. The field solution for a multilayer induction system is adapted to this case en Section II. In Section III the semianalytical model of forces is derived. Section IV presents the FEA verification of the model, and some experimental tests are described in Section V. Finally, some conclusions are summarized in Section VI.

## II. MAGNETIC FIELD DERIVATION

The fields involved in the induction system of Fig. 1 can be obtained by particularizing the semianalytical model of a planar coil between two multilayer media [36]. In this model the vector potential was obtained by solving the Poisson's equation and applying the Fourier-Bessel integral transform method. Therefore, the vector potential is expressed as definite integrals which are numerically solved.

The assumptions adopted to obtain the vector potential are as follows:

- Axial symmetry.
- Filamentary currents for the coil.
- Semiinfinite media in the horizontal dimension.
- Linear, homogeneous and isotropic materials. Therefore, saturation of ferromagnetic materials is not considered.
- Magneto-quasi-static approximation at the interest frequency range, from 20 kHz to 100 kHz.

The first four assumptions are requirements for obtaining an analytical solution. The magneto-quasi static approximation is valid if the dimensions of the system are lesser than the wavelength of the field at the higher frequency range. In this case, considering 100 kHz, the corresponding electromagnetic wavelength is about 3 km, whereas the typical dimension of cookers is about tens of centimeters. Linearity of the materials can be assumed if the temperature reached in the cooking process is below the Curie's temperature. The assumptions imposed by the analytical solution will be validated by means of an experimental verification.

The geometrical model for obtaining the fields of the induction system is presented in Fig. 2. In this model, the coil is placed at $z = 0$, and it consists of $n$ concentric filamentary currents of value $\hat{I}e^{j\omega t}$, where $\hat{I}$ is the amplitude and $\omega$ the angular frequency. Filamentary currents are placed between two multilayer media representing the air, the ferrite bars, the aluminum shielding and the pot. Ferrite bars and the existing air between them are modeled by means of a lossless flux concentrator layer with the same thickness of the bars and an equivalent magnetic relative permeability. The equivalent relative permeability is lesser than the relative permeability of ferrite bars and it is in between the relative permeability of the ferrite (about 1000) and the relative permeability of the air. The equivalent relative permeability is proportional to the volume occupied by ferrite bars with respect to the volume of a disk whose external radius coincides with the most external face of ferrites. At the interest frequency range the dissipative

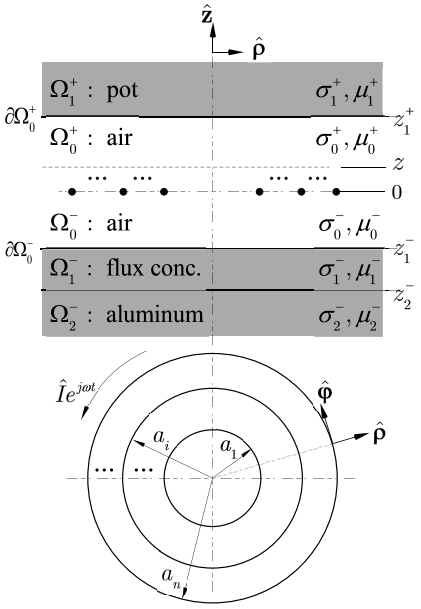


**FIGURE 2.** Geometry of the resolution model of the induction heating system.

media (i.e. the pot and the aluminum) can be considered as semiinfinite in the vertical direction due to the small skin depth of the fields compared with the usual thickness of these elements. At the lowest frequency of interest (i.e. 20 kHz) the skin depth of a typical ferromagnetic pot ($\sigma = 3 \cdot 10^6$ [S/m], $\mu_r = 250$) is 130 $\mu$m, and the skin depth of a typical aluminum ($\sigma = 2 \cdot 10^7$ [S/m], $\mu_r = 1$) is 800 $\mu$m. In contrast the thicknesses of these elements in typical applications can range from four or five millimeters up one or two centimeters.

Considering a point placed at $\mathbf{r}(\rho, z)$ of the domain $\Omega_0^+$, the vector potential is the sum of two contributions: the first, $\mathbf{A}_c$, corresponds to the coil in the air, and the second, $\Delta\mathbf{A}_m$, corresponds to the effect of the top and bottom multilayer media. The total magnetic vector potential at any point of the domain $\Omega_0^+$ is:

$$\mathbf{A}(\rho, z) = \mathbf{A}_c + \Delta\mathbf{A}_m \tag{1}$$

These contributions are, respectively [36]:

$$\mathbf{A}_c(\rho, z) = \frac{\mu_0 \hat{I}}{2} \int_0^\infty e^{-\beta z} J_1(\beta\rho)\, G(\beta a)\, d\beta \tag{2}$$

$$\Delta\mathbf{A}_m(\rho, z) = \frac{\mu_0 \hat{I}}{2} \int_0^\infty \Phi_A(z, \beta)\, J_1(\beta\rho)\, G(\beta a)\, d\beta \tag{3}$$

where $\beta$ is the integration variable of the Fourier-Bessel transform, $J_1$ is the Bessel function of first class and order 1. The function $G(\beta a_i)$ of (2) and (3) accounts for radii of the filamentary turns, and is defined as follows:

$$G(\beta a) = \sum_{i=1}^{n} J_1(\beta a_i) \tag{4}$$

The function $\Phi_A(z, \beta)$ includes the dependency of the vector potential with respect to the top and bottom multilayer

properties and thicknesses. This function is defined as follows:

$$\Phi_A(\beta, z) = \frac{\phi_t \left(e^{-\beta d_t} + \phi_b e^{-\beta(d_t - 2d_b)}\right) e^{-\beta(d_t - z)}}{1 - \phi_t \phi_b e^{-2\beta(d_t - d_b)}} + \frac{\phi_b \left(e^{-\beta d_b} + \phi_t e^{-\beta(2d_t - d_b)}\right) e^{-\beta(z - d_b)}}{1 - \phi_t \phi_b e^{-2\beta(d_t - d_b)}} \quad (5)$$

In this equation the following characteristic distances are used:

$$\begin{aligned} d_t &= z_1^+ \\ d_b &= z_1^- \end{aligned} \quad (6)$$

Functions $\phi_t$ and $\phi_b$ of (5) are characteristic of the properties and arrangement of the top and bottom multilayer media. In order to define these functions, the following parameter is required:

$$\eta_k^{\pm} = \left(\beta^2 + j\omega\sigma_k^{\pm}\mu_k^{\pm}\right)^{\frac{1}{2}} \quad (7)$$

where $\sigma_k^{\pm}$, $\mu_k^{\pm}$ are the electrical conductivity and magnetic permeability of the $k^{th}-$layer as it is shown in Fig. 2. Moreover, the thickness of the flux concentrator layer is defined as $t_f = z_1^- - z_2^-$. According to these definitions and the results of [36], for this particular case:

$$\phi_t = \frac{\beta\mu_{r1}^+ - \eta_1^+}{\beta\mu_{r1}^+ + \eta_1^+} \quad (8)$$

and

$$\phi_b = \frac{\left(\mu_{r1}^- - 1\right)\left(\beta + \mu_{r1}^-\eta_2^-\right)e^{-\beta t_f} + \left(\mu_{r1}^- + 1\right)\left(\beta - \mu_{r1}^-\eta_2^-\right)e^{\beta t_f}}{\left(\mu_{r1}^- + 1\right)\left(\beta + \mu_{r1}^-\eta_2^-\right)e^{-\beta t_f} + \left(\mu_{r1}^- - 1\right)\left(\beta - \mu_{r1}^-\eta_2^-\right)e^{\beta t_f}} \quad (9)$$

Considering (1), the electrical and magnetic field components are obtained by means of:

$$\begin{aligned} E_\varphi(\rho, z) &= -j\omega A_\varphi \\ &= -\frac{j\omega\mu_0\hat{I}}{2}\int_0^\infty \left[e^{-\beta z} + \Phi_A(\beta, z)\right] J_1(\beta\rho)\, G(\beta a)\, d\beta \end{aligned} \quad (10)$$

$$\begin{aligned} H_z(\rho, z) &= \frac{1}{\mu_0}\frac{1}{\rho}\partial_\rho\left(\rho A_\varphi\right) \\ &= \frac{\hat{I}}{2}\int_0^\infty \beta\left[e^{-\beta z} + \Phi_A(\beta, z)\right] J_0(\beta\rho)\, G(\beta a)\, d\beta \end{aligned} \quad (11)$$

and

$$\begin{aligned} H_\rho(\rho, z) &= \frac{1}{\mu_0}\partial_z A_\varphi \\ &= -\frac{\hat{I}}{2}\int_0^\infty \beta\left[e^{-\beta z} - \Phi_B(\beta, z)\right] J_1(\beta\rho)\, G(\beta a)\, d\beta \end{aligned} \quad (12)$$

where

$$\Phi_B(\beta, z) = \frac{\phi_t \left(e^{-\beta d_t} + \phi_b e^{-\beta(d_t - 2d_b)}\right) e^{-\beta(d_t - z)}}{1 - \phi_t \phi_b e^{-2\beta(d_t - d_b)}} - \frac{\phi_b \left(e^{-\beta d_b} + \phi_t e^{-\beta(2d_t - d_b)}\right) e^{-\beta(z - d_b)}}{1 - \phi_t \phi_b e^{-2\beta(d_t - d_b)}} \quad (13)$$

The precedent fields are used for calculating the force in the cookware. Moreover, these fields can be also used for obtaining the delivered power by means of the Poynting's vector, $\mathbf{S} = \mathbf{E} \times \mathbf{H}$, which represents the electromagnetic energy density flowing through a surface. In this case, the power density at the bottom of the cookware is:

$$p(\rho, z) = E_\varphi(\rho, z) \times H_\rho(\rho, z) \quad (14)$$

The power density is not uniformly distributed at the bottom of the cookware and this distribution is determined by the geometry of planar coils with equally-spaced turns. Fig. 3 shows the typical power density distribution at the bottom of the pot for the mentioned case of and equally-spaced turn coil. This fact is also reflected in the distribution of the vertical force.

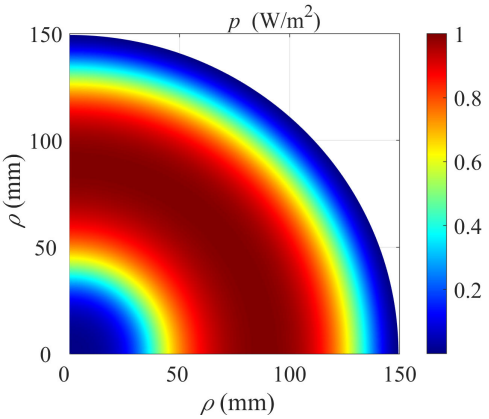


**FIGURE 3.** Power density distribution at the bottom of the cookware.

## III. ANALYTICAL CALCULATION OF VERTICAL FORCES ON THE COOKWARE

Skin depth of varying fields in a material ($\delta = \sqrt{2/\omega\sigma\mu}$) is determinant in the induction heating process. The inductive heating of ferromagnetic cookware is mainly due to intense induced currents, which are confined at the bottom surface in a layer of tens of microns. Additionally, magnetic hysteresis and its corresponding dissipation also occurs in the layer penetrated by the fields. Consequently, the induction heating of ferromagnetic materials combines both current density and magnetization, and these phenomena interact with the field created by the coil generating two opposite forces: repulsive force caused by the interaction between the driven and the induced current, and attractive force due to magnetization of the material. In this case, the Maxwell's stress tensor is chosen for calculating the net force. This option shows some advantages, for example, current densities are not involved in calculations and only fields **E** and **H** are required.

In this case the Maxwell 's stress tensor is a 3 × 3 rank-2 tensor whose $ij^{th}$ element is given by:

$$\mathbb{T}_{ij}(\rho, z) = \varepsilon_0 \left( E_i E_j - \frac{1}{2}\delta_{ij} E^2 \right) + \frac{1}{\mu_0} \left( B_i B_j - \frac{1}{2}\delta_{ij} B^2 \right) \quad i, j = \rho, z, \varphi \tag{15}$$

where $\delta_{ij}$ is the Kronecker delta. Considering in this case sinusoidal sources, the average value of the $\mathbb{T}_{zz}$ in a point of the domain $\Omega_0^+$ is:

$$\mathbb{T}_{zz\_avg}(\rho, z) = \frac{1}{4}\left[ \varepsilon_0 \left( -E_\varphi E_\varphi^* \right) + \mu_0 \left( H_z H_z^* - H_r H_r^* \right) \right] \tag{16}$$

where the asterisk denotes a complex conjugated magnitude. The following expression connects the stress tensor and the force density:

$$\mathbf{f} + \underbrace{\varepsilon_0 \mu_0 \frac{\partial \mathbf{S}}{\partial t}}_{0} = \nabla \cdot \mathbb{T} \tag{17}$$

where the term dependent of the Poynting's vector is neglected due to adopted magneto-quasi-static approximation. The force is obtained by integrating the force density at the interest domain volume, or alternatively, applying the divergence theorem, the force is obtained by integrating the stress tensor at the bounding surface. This surface is denoted as $\partial\Omega_0^+$ in Fig. 2. Therefore, the average vertical force exerted on the cookware is:

$$F_{z\_avg} = \int_{\Omega_0^+} f_{z\_avg} dv = \int_{\partial\Omega_0^+} \mathbb{T}_{zz\_avg} ds \tag{18}$$

Considering (16), the force calculation involves the surface integrals of the product of a field and its conjugate at the points $(\rho, z = d_t)$. Therefore the aspect of these integrals is:

$$2\pi \int_0^\infty M_\alpha(\rho, d_t) M_\alpha^*(\rho, d_t) \cdot \rho \cdot d\rho \tag{19}$$

where $M_\alpha$ can be $E_\varphi$, $H_z$ or $H_\rho$. Taking into account the field definitions of (10), (11) and (12), the conjugate applies only to functions $\Phi_A(\beta, d_t)$ and $\Phi_B(\beta, d_t)$. Moreover, the Fourier-Bessel integration variables $\beta$ and $\beta'$ are adopted for a field and its conjugate, respectively. Additionally, considering the so called *closure equations* of integrals involving products of Bessel functions [38]:

$$\int_0^\infty \rho J_n(\rho\beta) J_n(\rho\beta') d\rho = \frac{1}{\beta}\delta(\beta - \beta') \quad n = 0, 1 \tag{20}$$

where $\delta(\beta - \beta')$ is the Dirac delta function, the following results are obtained:

$$2\pi \int_0^\infty E_\varphi(\rho, d_t) E_\varphi^*(\rho, d_t) \rho d\rho = -\pi \mu_0^2 \omega^2 \frac{\hat{I}^2}{2} \times \int_0^\infty \frac{1}{\beta} \left[ e^{-\beta d_t} + \Phi_A(\beta, d_t) \right] \times \left[ e^{-\beta d_t} + \Phi_A^*(\beta, d_t) \right] G^2(\beta a) d\beta \tag{21}$$

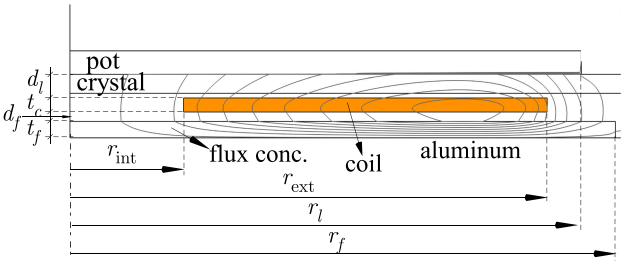


**FIGURE 4.** 2D simulation of the induction heating system. The current density of the coil and flux density lines are represented for illustrative purposes.

$$2\pi \int_0^\infty H_z(\rho, d_t) H_z^*(\rho, d_t) \rho d\rho = \pi \frac{\hat{I}^2}{2} \times \int_0^\infty \beta \left[ e^{-\beta d_t} + \Phi_A(\beta, d_t) \right] \times \left[ e^{-\beta d_t} + \Phi_A^*(\beta, d_t) \right] G^2(\beta a) d\beta \tag{22}$$

$$2\pi \int_0^\infty H_\rho(\rho, d_t) H_\rho^*(\rho, d_t) \rho d\rho = \pi \frac{\hat{I}^2}{2} \times \int_0^\infty \beta \left[ e^{-\beta d_t} - \Phi_B(\beta, d_t) \right] \times \left[ e^{-\beta d_t} - \Phi_B^*(\beta, d_t) \right] G^2(\beta a) d\beta \tag{23}$$

Expressions (21), (22), (23) only involve an integral, as occurs in the case of the equations (10), (11), (12) of the fields. At the interest frequency range (21) is much smaller than (22) and (23). Moreover, at sinusoidal regime it holds that $\hat{I}^2 \big/ 2 = I_{rms}^2$.

## IV. FINITE ELEMENT VALIDATION

In order to validate the derived models of fields and force, (10), (11) and (12), (21), (22) and (23) are implemented in MATLAB and results are compared with 2D axisymmetric FEA simulations by means of COMSOL. An image of the simulated system is shown in Fig. 4, where the current density of the coil and some magnetic flux density lines are also shown for illustrative purposes. This structure basically corresponds to the geometrical model of Fig. 2, except for the following aspects:

- The coil of filamentary currents is replaced by an ideal rectangular cross-sectional constant current density of value $J_{\text{i}} = n\hat{I} \big/ h_{\text{i}}(r_{\text{ext}} - r_{\text{int}})$.
- Dissipative media (aluminum and pot) are considered as an Impedance Boundary Condition (IBC) for the resolution. In the case of the aluminum, the domain is directly replaced by the IBC condition. However, the domain of the pot is part of the resolution system due to its finite radius, and the IBC condition is applied to the bottom boundary of the domain.

The first assumption is essentially valid in the case of coils with high density of turns, as occurs in commercial applications. The second is valid if the skin depth of fields is

lesser than the thickness of the domain, which is the case of both cookware and aluminum, as was previously discussed.

The dimensions and parameters the geometry of both semi-analytical and FEA models are listed in Table 1 and Table 2, respectively.

**TABLE 1. Parameters of the analytical model.**

| Description | Symbol | Value | Units |
|---|---|---|---|
| Number of turns | $n$ | 17 | [-] |
| Internal radius | $a_1$ | 25 | [mm] |
| External radius | $a_{17}$ | 105 | [mm] |
| Coordinate of the top media | $z_1^+$ | 6.5 | [mm] |
| Coordinate of the bottom media | $z_1^-$ | -3.5 | [mm] |
| Flux concentrator thickness | $t_f$ | 3.5 | [mm] |

**TABLE 2. Parameters of the FEA model.**

| Description | Symbol | Value | Units |
|---|---|---|---|
| Internal radius | $r_{int}$ | 25 | [mm] |
| External radius | $r_{ext}$ | 105 | [mm] |
| Distance coil-pot | $d_l$ | 5 | [mm] |
| Coil thickness | $t_c$ | 3 | [mm] |
| Distance coil-flux concentrator | $d_f$ | 2 | [mm] |
| Pot radius | $r_l$ | 150 | [mm] |
| Flux concentrator radius | $r_f$ | 170 | [mm] |

The material properties and current level required for the validation are set according to the experimental tests of the next section. Two different materials, Material A and Material B are used for comparing calculated and simulated results. These materials are typically used in the available cookware and represents two cases of ferromagnetic materials with different resistivity. The properties of these materials, and the others involved in the system are presented in Table 3. As it is shown in this Table, both materials have similar permeability. In order to improve the thermal stability of the system, the cookware is filled with water in the experiments. For this reason, the properties are estimated for the boiling water condition, i.e. $T = 100\,^{\circ}\text{C}$. On the other hand, the equivalent relative magnetic permeability of the flux concentrator disk is obtained by comparing the measured inductance of the planar coil in the air with respect to the case of the ferrite bars [14].

**TABLE 3. Properties of materials.**

| Description | Symbol | Value | Units |
|---|---|---|---|
| Material A conductivity | $\sigma$ | $1 \cdot 10^7$ | [S/m] |
| Material A rel. permeability | $\mu_r$ | 250 | [-] |
| Material B conductivity | $\sigma$ | $3 \cdot 10^6$ | [S/m] |
| Material B rel. permeability | $\mu_r$ | 250 | [-] |
| Flux concentrator conductivity | $\sigma$ | 0 | [S/m] |
| Flux concentrator rel. permeability | $\mu_r$ | 5 | [-] |
| Aluminum conductivity | $\sigma$ | $2 \cdot 10^7$ | [S/m] |
| Aluminum. rel. permeability | $\mu_r$ | 1 | [-] |

The rms current for materials A and B is set to 30 and 28 A, respectively. These currents correspond to the rated power for this inductor size with ferromagnetic materials, i.e. $P_o = 2200$ W. The current for the Material A is higher than the current for the Material B because its equivalent impedance is lesser, corresponding to its lesser resistivity.

Calculated and simulated results of fields $E_\phi$, $H_r$, $H_z$ are shown in Fig. 5, Fig. 6, Fig. 7. These magnitudes are evaluated at the bottom surface of the pot and they are represented with respect to the radial coordinate. As it can be observed, the agreement between calculated and simulated results is, in general, good. Discrepancies could be caused for the different model of the coil adopted between both analytical and FEA resolutions.

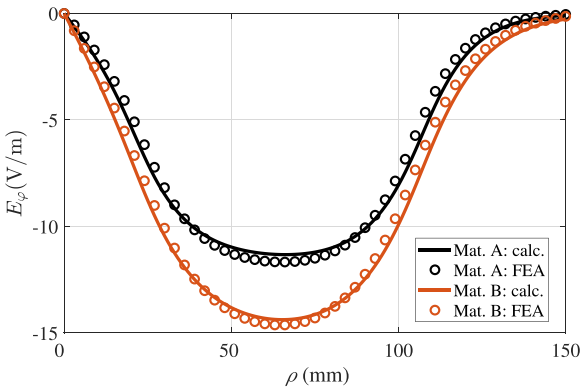


**FIGURE 5. Calculated and simulated electrical field with respect to the radial coordinate of the bottom boundary of the cookware.**

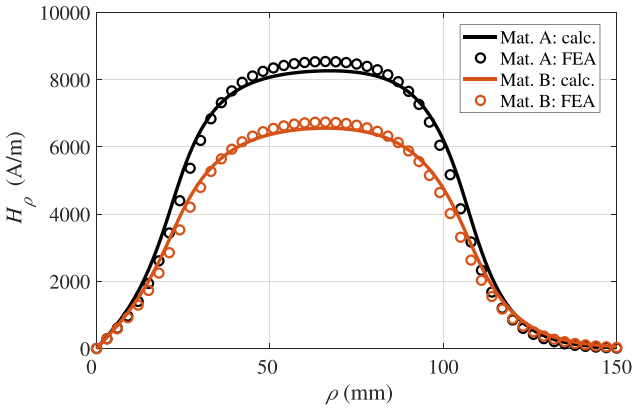


**FIGURE 6. Calculated and simulated radial component of the magnetic field with respect to the radial coordinate of the bottom boundary of the cookware.**

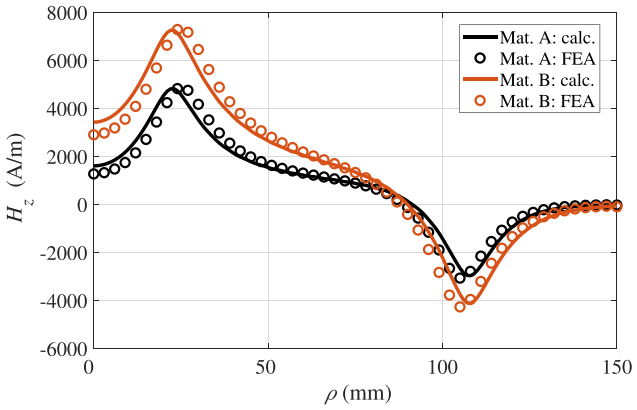


**FIGURE 7.** Calculated and simulated vertical component of the magnetic field with respect to the radial coordinate of the bottom boundary of the cookware.

The magnitude $\mathbb{T}_{zz\_avg}$ is evaluated by means of (16) and the results are compared with FEA simulations in Fig. 8. This magnitude has two signs corresponding to the different directions of the force, which depends on the radial coordinate. The negative sign corresponds to repulsive force. The global force is obtained by means of (18) and (21), (22) and (23) and results are presented in Table 4.

**TABLE 4.** Calculated and simulated global force.

| | Material A | Material B | Units |
|---|---|---|---|
| Calculated | $-0.556$ | $-0.265$ | [N] |
| Simulated | $-0.581$ | $-0.271$ | [N] |

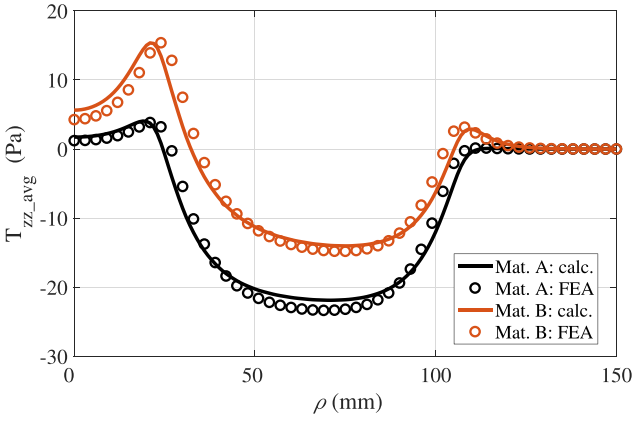


**FIGURE 8.** Calculated and simulated vertical component of the average stress tensor with respect to the radial coordinate of the bottom boundary of the cookware.

The model also captures the dependency on the force with respect to the frequency. This dependency reflects the fact that induced currents are dependent of the frequency and the material properties. This result is relevant because the in usual arrangements the power supplied to the cookware is controlled by means of the frequency. Simulated and calculated forces with respect to frequency are shown in Fig. 9. As it can be observed, at low frequencies the net force is attractive because the magnetization effect is predominant. However, at the higher frequency range, eddy currents are predominant and the resultant force is repulsive. In general, the observed agreement is good, in concordance with the results obtained for the fields.

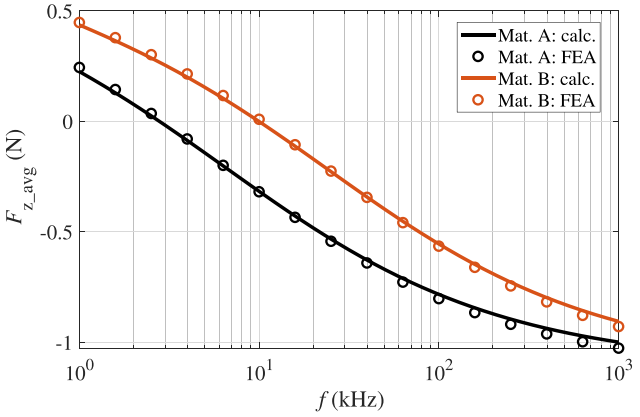


**FIGURE 9.** Calculated and simulated vertical force with respect to the frequency.

Is also worth to compare the computational cost required for obtaining Fig. 5, Fig. 6, Fig. 7 with the developed model and a FEA simulation. The same platform was used in this comparison and it consisted of a basic computer with an Intel$^{TM}$ Core i7 at 3.6GHz and 32 GB of RAM memory. The analytical model was conveniently parameterized and implemented in Matlab and the used FEA tool was COMSOL. The CPU time required to calculate the results shown in the precedent figures was 0.055 s whereas the time required by the FEA tool (considering a mesh with 7059 elements) was 2.8 s. Apart form these results, in the case of systematic analysis with respect to geometrical parameters, the FEA tool requires redrawn each new geometry whereas the analytical model just needs to change some parameters.

## V. EXPERIMENTAL TESTS

Some experimental tests are carried out with the purpose of qualitatively verify the developed model and simulations. Rather than a systematic verification, the objective of experiments is to measure the force in typical cooking experiences and to compare the measurements with the developed semi-analytical model and simulations.

The experimental setup is based on a commercial induction heating appliance and commercial pots, whose properties are shown in the previous section. The appliance is connected to the mains and its nominal rated power for ferromagnetic pots is $P_o = 2200$ W. The pot-cooker set is resting on three load cells (Fig. 10) whose measurements are captured by means of a Yokogawa MW100 data logger. An image of the experimental setup is shown in Fig. 11.

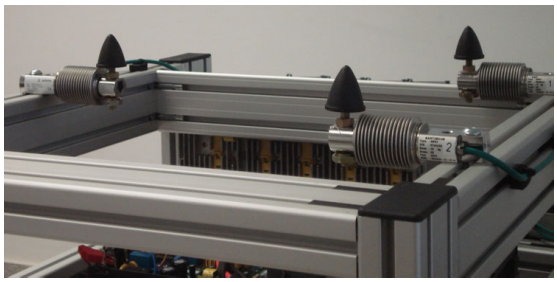

**FIGURE 10.** Image of the experimental weighting system based on three load cells.

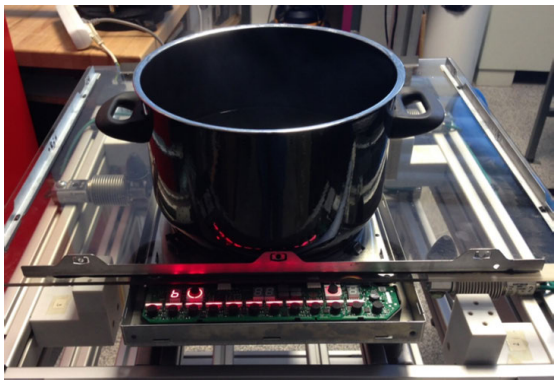

**FIGURE 11.** Image of the experimental setup.

Experiments are described as follows. Water is added in the pot until the weight of the set is 78.48 N, (8 kg). This water is preheated just before the boiling point and, at this moment, the heating is turned off and the weight is started to be recorded. Few seconds after, the heating at nominal power is turned on and the weight experiments a sharp change. This change can be observed if the heating is turned-on turned-off several times. When the boiling regime is reached, an smooth drop of the weight is observed.

The weight recorded during this process is presented in Fig. 12 for the Material A and Fig. 13 for the Material B. As it is shown in these figures, the measured change of the

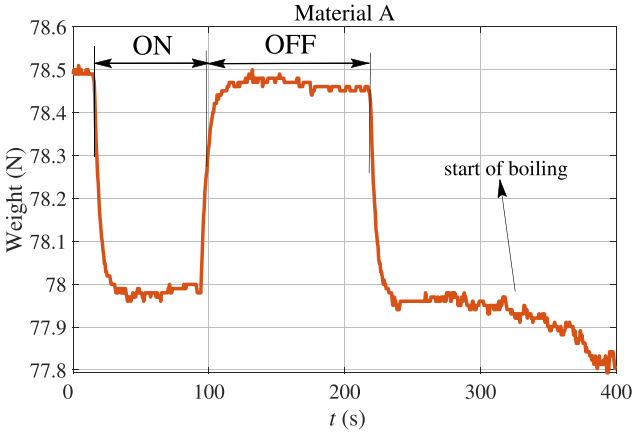


**FIGURE 12.** Experimental results corresponding to the Material A.

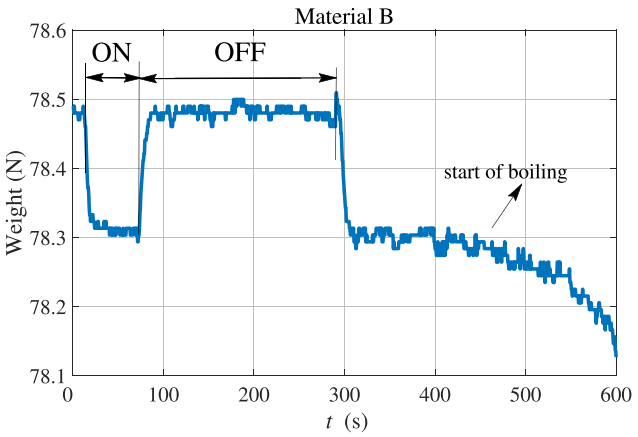


**FIGURE 13.** Experimental results corresponding to the Material B.

weigh was 0.510 N and 0.192 N. Comparing with the results of the Table 4 an acceptable agreement is also observed.

## VI. CONCLUSION

In this work, a two-dimensional semianalytical solution for calculating the forces on cookware heated by domestic induction heating appliances is presented. The model is original for this application and is based on the analytical solution of the fields generated by a planar coil in a stratified media. The forces are obtained by integrating the Maxwell's stress tensor, which is obtained by means of the mentioned fields. This approach captures the combination of electromechanical and dissipative regimes of the cookware in induction heating applications. This regime is specific of this application and is not found in other electromechanical applications, as electrical machines, where usually magnetic and electrical paths are different. The model includes the dependencies with respect to the excitation current, the system geometry, the operating frequency and the properties of the materials of the system. The analytical model is implemented in Matlab and results are compared with finite element simulations. In general, both calculated and simulated results show good agreement. However, the analytical model takes less computation time and also reduces the development time required by finite element tools for implementing the analysis of the influence of the system geometry on the forces.

Additionally, the model is also checked by means of experimental results. Forces on the cookware are reflected in a change of the weight, and this change could interfere with the automatic cooking functionalities of modern appliances. Weighting experiments are carried out and measurements also shows good agreement with numerical results for two different materials.

Summarizing, this work contributes an original analytical model for an application with a rich physical insight, different from other electromechanical systems. The observed advantages of the analytical model with respect to finite element simulations, as computational time savings and flexibility for systematic parameterized analysis, makes it suitable for analyzing the considered systems.

## REFERENCES

[1] J. Acero, J. Burdío, L. Barragán, D. Navarro, R. Alonso, J. García, F. Monterde, P. Hernández, and S. L. I. Garde, "Domestic induction appliances," *IEEE Ind. Appl. Mag.*, vol. 16, no. 2, pp. 39–47, Mar. 2010.
[2] I. Lope, C. Carretero, J. Acero, R. Alonso, and J. M. Burdío, "Frequency-dependent resistance of planar coils in printed circuit board with Litz structure," *IEEE Trans. Magn.*, vol. 50, no. 12, pp. 1–9, Dec. 2014.
[3] C. Carretero, J. Acero, R. Alonso, and J. M. Burdío, "Normal-mode decomposition of surface power distribution in multiple-coil induction heating systems," *IEEE Trans. Magn.*, vol. 52, no. 2, pp. 1–8, Feb. 2016.
[4] W. Han, K. T. Chau, Z. Zhang, and C. Jiang, "Single-source multiple-coil homogeneous induction heating," *IEEE Trans. Magn.*, vol. 53, no. 11, pp. 1–6, Nov. 2017.
[5] W. Han, K. T. Chau, C. Jiang, and W. Liu, "All-metal domestic induction heating using single-frequency double-layer coils," *IEEE Trans. Magn.*, vol. 54, no. 11, pp. 1–5, Nov. 2018.
[6] V. T. Kilic, E. Unal, N. Yilmaz, and H. V. Demir, "All-surface induction heating with high efficiency and space invariance enabled by arraying squircle coils in square lattice," *IEEE Trans. Consum. Electron.*, vol. 64, no. 3, pp. 339–347, Aug. 2018.
[7] J. Serrano, I. Lope, and J. Acero, "Nonplanar overlapped inductors applied to domestic induction heating appliances," *IEEE Trans. Ind. Electron.*, vol. 66, no. 9, pp. 6916–6924, Sep. 2019.
[8] S. Komeda and H. Fujita, "A phase-shift-controlled direct AC-to-AC converter for induction heaters," *IEEE Trans. Power Electron.*, vol. 33, no. 5, pp. 4115–4124, May 2018.
[9] H. Sarnago, P. Guillén, J. M. Burdío, and O. Lucía, "Multiple-output ZVS resonant inverter architecture for flexible induction heating appliances," *IEEE Access*, vol. 7, pp. 157046–157056, 2019.
[10] R. C. M. Gomes, M. A. Vitorino, D. A. Acevedo-Bueno, and M. B. D. R. Correa, "Multiphase resonant inverter with coupled coils for AC–AC induction heating application," *IEEE Trans. Ind. Appl.*, vol. 56, no. 1, pp. 551–560, Jan. 2020.
[11] N. Domingo, L. A. Barragán, J. M. M. Montiel, A. Domínguez, and J. I. Artigas, "Fast power–frequency function estimation for induction heating appliances," *Electron. Lett.*, vol. 53, no. 7, pp. 498–500, Mar. 2017.
[12] J. Villa, J. I. Artigas, J. R. Beltrán, A. D. Vicente, and L. A. Barragán, "Analysis of the acoustic noise spectrum of domestic induction heating systems controlled by phase-accumulator modulators," *IEEE Trans. Ind. Electron.*, vol. 66, no. 8, pp. 5929–5938, Aug. 2019.
[13] T. Shimotani, H. Igarashi, E. Hashimoto, and H. Imanari, "Equivalent circuit allowing loss separation synthesized from field computations: Application to induction heating," *IEEE Trans. Magn.*, vol. 56, no. 2, pp. 1–5, Feb. 2020.
[14] J. Acero, C. Carretero, R. Alonso, and J. M. Burdío, "Quantitative evaluation of induction efficiency in domestic induction heating applications," *IEEE Trans. Magn.*, vol. 49, no. 4, pp. 1382–1389, Apr. 2013.
[15] O. Lucia, D. Navarro, P. Guillén, H. Sarnago, and S. Lucía, "Deep learning-based magnetic coupling detection for advanced induction heating appliances," *IEEE Access*, vol. 7, pp. 181668–181677, 2019.
[16] S. Lucía, D. Navarro, B. Karg, H. Sarnago, and O. Lucía, "Deep learning-based model predictive control for resonant power converters," *IEEE Trans. Ind. Informat.*, early access, Jan. 27, 2020, doi: 10.1109/TII.2020.2969729.
[17] K. Kamaeguchi, K. Umetani, and E. Hiraki, "Axial heating coil structure for reducing magnetic levitation force of all-metal type induction cookers," in *Proc. 8th Int. Conf. Renew. Energy Res. Appl. (ICRERA)*, Nov. 2019, pp. 793–798.
[18] C. M. Zingerli, T. Nussbaumer, and J. W. Kolar, "Optimizing repulsive lorentz forces for a levitating induction cooker," *IEEJ J. Ind. Appl.*, vol. 4, no. 4, pp. 439–444, 2015.
[19] R. Pile, E. Devillers, and J. Le Besnerais, "Comparison of main magnetic force computation methods for noise and vibration assessment in electrical machines," *IEEE Trans. Magn.*, vol. 54, no. 7, pp. 1–13, Jul. 2018.
[20] J. Kitao, Y. Takahashi, K. Fujiwara, A. Ahagon, T. Matsuo, and A. Daikoku, "Input and output power in finite-element analysis of electric machines taking account of hysteretic property," *IEEE Trans. Magn.*, vol. 54, no. 3, pp. 1–4, Mar. 2018.
[21] V. Rallabandi, J. Wu, P. Zhou, D. G. Dorrell, and D. M. Ionel, "Optimal design of a switched reluctance motor withmagnetically disconnected rotor modules usinga design of experiments differential evolution FEA-based method," *IEEE Trans. Magn.*, vol. 54, no. 11, Nov. 2018, Art. no. 8205705.
[22] K. N. Jenney and S. Pakdelian, "Leakage flux of the trans-rotary magnetic gear," *IEEE Trans. Magn.*, vol. 55, no. 7, pp. 1–8, Jul. 2019.
[23] L. Qiu, Y. Li, Y. Yu, A. Abu-Siada, Q. Xiong, X. Li, L. Li, P. Su, and Q. Cao, "Electromagnetic force distribution and deformation homogeneity of electromagnetic tube expansion with a new concave coil structure," *IEEE Access*, vol. 7, pp. 117107–117114, 2019.
[24] L. Qiu, N. Yi, A. Abu-Siada, J. Tian, Y. Fan, K. Deng, Q. Xiong, and J. Jiang, "Electromagnetic force distribution and forming performance in electromagnetic forming with discretely driven rings," *IEEE Access*, vol. 8, pp. 16166–16173, 2020.
[25] L. Qiu, W. Zhang, A. Abu-Siada, Q. Xiong, C. Wang, Y. Xiao, B. Wang, Y. Li, J. Jiang, and Q. Cao, "Electromagnetic force distribution and wall thickness reduction of three-coil electromagnetic tube bulging with axial compression," *IEEE Access*, vol. 8, pp. 21665–21675, 2020.
[26] L. Qiu, W. Zhang, A. Abu-Siada, G. Liu, C. Wang, Y. Wang, B. Wang, Y. Li, and Y. Yu, "Analysis of electromagnetic force and formability of tube electromagnetic bulging based on convex coil," *IEEE Access*, vol. 8, pp. 33215–33222, 2020.
[27] J. Acero, C. Carretero, I. Lope, and J. M. Burdío, "An analysis of electromagnetic forces on cooking vessels used in domestic induction heating appliances oriented to identify the properties of materials," in *Proc. IEEE Appl. Power Electron. Conf. Expo. (APEC)*, Mar. 2019, pp. 1971–1975.
[28] J. L. G. Janssen, J. J. H. Paulides, and E. A. Lomonova, "3-D analytical calculation of the torque between perpendicular magnetized magnets in magnetic suspensions," *IEEE Trans. Magn.*, vol. 47, no. 10, pp. 4286–4289, Oct. 2011.
[29] K. J. Meessen, J. J. H. Paulides, and E. A. Lomonova, "Force calculations in 3-D cylindrical structures using Fourier analysis and the Maxwell stress tensor," *IEEE Trans. Magn.*, vol. 49, no. 1, pp. 536–545, Jan. 2013.
[30] Z. Andjelic, K. Ishibashi, C. Lage, and P. Di Barba, "On a study of magnetic force evaluation by double-layer approach," *IEEE Trans. Magn.*, vol. 56, no. 2, pp. 1–5, Feb. 2020.
[31] R. Pile, Y. Le Menach, J. Le Besnerais, and G. Parent, "Study of the combined effects of the air-gap transfer for Maxwell tensor and the tooth mechanical modulation in electrical machines," *IEEE Trans. Magn.*, vol. 56, no. 1, pp. 1–4, Jan. 2020.
[32] Z. Li, D. Wang, and D. Zheng, "Accurate prediction and analysis of electromagnetic fields and forces in flux-focusing eddy current coupling with double slotted conductor rotors," *IEEE Access*, vol. 6, pp. 37685–37699, 2018.
[33] W. G. Shadid and R. Shadid, "The electric origin of magnetic forces theory: General framework," *IEEE Access*, vol. 8, pp. 73756–73766, 2020.
[34] F. Dughiero, S. Lupi, and P. Siega, "Calculation of forces in travelling wave induction heating systems," *IEEE Trans. Magn.*, vol. 31, no. 6, pp. 3560–3562, Nov. 1995.
[35] H. Li, S. Wang, H. He, Y. Huangfu, and J. Zhu, "Electromagnetic-thermal–deformed-fluid-coupled simulation for levitation melting of titanium," *IEEE Trans. Magn.*, vol. 52, no. 3, pp. 1–4, Mar. 2016.
[36] J. Acero, R. Alonso, L. A. Barrágan, and J. M. Burdío, "Modeling of planar spiral inductors between two multilayer media for induction heating applications," *IEEE Trans. Magn.*, vol. 42, no. 11, pp. 3719–3729, Nov. 2006.
[37] J. Acero, R. Alonso, J. M. Burdío, L. A. Barragan, and D. Puyal, "Analytical equivalent impedance for a planar circular induction heating system," *IEEE Trans. Magn.*, vol. 42, no. 1, pp. 84–86, Jan. 2006.
[38] G. B. Arfken and H. J. Weber, *Mathematical Methods for Physicists*, 4th ed. New York, NY, USA: Academic, 1995.

**JESÚS ACERO** (Senior Member, IEEE) received the M.Sc. and Ph.D. degrees in electrical engineering from the University of Zaragoza, Zaragoza, Spain, in 1992 and 2005, respectively. From 1992 to 2000, he was with several industry projects, especially focused on custom power supplies for research laboratories. In 2000, he was with the Department of Electronic Engineering and Communications, University of Zaragoza, where he is currently a Professor. His main research interests include resonant converters for induction heating applications, inductive-type load modeling, and electromagnetic modeling. He is a member of the IEEE Power Electronics, the Industrial Electronics, and the Magnetics Societies. He is also a member of the Instituto de Investigación en Ingeniería de Aragón (I3A).

**IGNACIO LOPE** (Member, IEEE) received the M.Sc. degree in electrical engineering and the Ph.D. degree in power electronics from the University of Zaragoza, Zaragoza, Spain, in 2010 and 2015, respectively. He is currently with BSH Home Appliances, Zaragoza, where he is involved in several projects focusing on developing domestic induction heating appliances. His current research interests include electromagnetic modeling of inductive coupled contactless energy transfer systems and loss modeling of magnetic devices.

**CLAUDIO CARRETERO** (Senior Member, IEEE) received the B.Sc. and M.Sc. degrees in physics, the B.Sc. and M.Sc. degrees in electrical engineering, and the Ph.D. degree in electrical engineering from the University of Zaragoza, Zaragoza, Spain, in 1998, 2002, and 2010, respectively. He is currently an Assistant Professor with the Department of Applied Physics, University of Zaragoza. His research interests include induction heating applications and electromagnetic modeling of inductive systems. He is a member of the Instituto de Investigación en Ingeniería de Aragón (I3A).

**JOSÉ M. BURDÍO** (Senior Member, IEEE) received the M.Sc. and Ph.D. degrees in electrical engineering from the University of Zaragoza, Zaragoza, Spain, in 1991 and 1995, respectively.

In 2000, he was a Visiting Professor with the Center for Power Electronics Systems, Virginia Tech. He was with the Department of Electronic Engineering and Communications, University of Zaragoza, where he is currently a Professor, the Head of the Group of Power Electronics and Microelectronics, and the Director of the BSH Power Electronics Laboratory. He is the author of more than 80 international journal articles and over 200 papers in conference proceedings. He holds more than 60 international patents. His main research interests include modeling of switching converters, resonant power conversion for induction heating, and biomedical applications. He is a Senior Member of the Power Electronics and the Industrial Electronics Societies. He is also a member of the Instituto de Investigación en Ingeniería de Aragón (I3A).